

Adsorption of oxygen on Pt₃Sn(110) studied by STM and LEED

M. Hoheisel* and S. Speller

Research Institute for Molecules and Materials, Radboud University Nijmegen, 6525 ED Nijmegen, The Netherlands

A. Atrei

Dipartimento di Scienze e Tecnologie Chimiche e dei Biosistemi, Università di Siena, 53100 Siena, Italy

U. Bardi and G. Rovida

Dipartimento di Chimica, Università di Firenze, 50019 Firenze, Italy

(Received 2 July 2003; revised manuscript received 8 September 2004; published 18 January 2005)

The adsorption of oxygen on the Pt₃Sn(110) alloy surface was studied by means of scanning tunneling microscopy (STM) and low-energy electron diffraction (LEED). After exposure to 2300 L O₂ at 750 K LEED shows additional $c(2 \times 2)$ spots with regard to the substrate $p(2 \times 1)$ pattern. This agrees straightforward with STM topographies revealing a thin layer of large protrusions, arranged in a pseudo-hexagonal lattice. This layer is split into domains separated by distinctive zigzagging boundaries. Post-annealing allowed to partially uncover substrate regions. That way it could be shown that the protrusions are located above Sn locations. Further post-annealing restored the original substrate completely. A model of the adlayer structure consistent with all STM and LEED findings is given. These features observed after high temperature oxygen exposure of the Pt₃Sn(110) surface resemble to a large extent structures obtained on the Pt₃Sn(111) surface under similar conditions. The observed structures can be understood in terms of Sn-O entities interacting with each other. However, results from the oxidation of Pt₃Sn(111) indicate the formation of a Sn layer with chemisorbed oxygen on top, but not of separated SnO_x entities. The protrusion patterns observed with STM on both surfaces are a topographic signature of such Sn-O layers on Pt₃Sn.

DOI: 10.1103/PhysRevB.71.035410

PACS number(s): 68.47.De, 68.37.Ef, 61.14.Hg, 81.65.Mq

I. INTRODUCTION

The compositional and structural characterization of the phases formed upon oxygen exposure of Pt-Sn alloy surfaces is interesting from the point of view of the surface chemistry of this bimetallic system. Surfaces containing Pt and Sn are useful for hydrocarbon conversion as well as for the electro-oxidation of methanol in fuel cells.¹⁻³ Tin oxide layers are expected to form on Pt-Sn surfaces upon exposure to O₂, as tin has a higher affinity toward oxygen than platinum. Changes of the surface region composition occurring after oxygen exposure can modify substantially the functional properties of the alloy surface, in particular the chemical reactivity. Moreover, the study of the interaction of oxygen with Pt-Sn alloy surfaces is relevant considering the role of platinum in promoting the selectivity and sensitivity of gas sensors based on SnO₂.⁴

Hoflund *et al.* investigated the oxidation⁵⁻⁸ and reduction⁹ of polycrystalline Pt₃Sn surfaces. Upon oxidation segregation of Sn to the surface was observed, the surface Pt concentration decreased. A tin oxide overlayer is formed on top of a Pt-rich region. Electron spectroscopy for chemical analysis (ESCA) [x-ray photoelectron spectroscopy (XPS)] indicated oxidation of the Sn in the outermost surface region but no change in the Pt core-level features. It was reported that on the polycrystalline samples Sn mainly segregates through grain boundaries.⁶ Maximal oxygen uptake occurred at a dosing temperature of 470 K.⁸ While then two forms of oxygen were present, assigned to be oxidic and adsorbed oxygen, only an oxidic form was present after dosing at 670 K. In a secondary ion mass spectrometry (SIMS) and

XPS examination of low-pressure oxygen adsorption on polycrystalline Pt₃Sn Unger and Marton¹⁰ concluded that the oxygen uptake of Pt₃Sn increases monotonically up to ~800 K. At elevated temperatures ($500 \leq T \leq 800$ K) oxygen incorporation accompanied by a formation of an “oxidic” phase as proposed by Hoflund *et al.* was found.

Recently the oxidation of Pt₃Sn(111) alloy surface^{11,12} and of Sn-Pt(111) surface alloy¹³⁻¹⁷ single crystals has been studied. Both systems behave similar upon oxygen exposure: a very thin Sn-O layer is formed that is comprised of only a few atomic layers. Upon exposure at elevated temperatures a (4×4) superstructure is observed both with scanning tunneling microscopy (STM) and lowenergy electron diffraction (LEED). A test of structural models for this (4×4) phase formed by oxygen adsorption on Pt₃Sn(111) was performed by comparing LEED *I-V* curves with tensor LEED calculations.¹² The best agreement was obtained with a model in which the protrusions observed in STM would correspond to tin atoms occupying on-top positions.

In this study the oxidation experiments are extended to the Pt₃Sn(110) surface. Although it has not been studied in as much detail as the Pt₃Sn(111) surface (Ref. 18, and references therein), the general properties of the clean Pt₃Sn(110) alloy surface are well known.¹⁹⁻²² Similar to other Pt₃Sn low index surfaces sputtering of Pt₃Sn(110) causes a depletion of the surface region in Sn. After annealing at 600 K low-energy ion sputtering (LEIS) and auger electron spectroscopy (AES) indicate a Sn-rich outermost layer above a Pt-rich subsurface region. STM topographies of this metastable regime show a distinct hill-and-valley structure consisting

mainly of $\{102\}$ facets.²² The previously reported ambiguous LEED patterns²¹ are due to facet spots. After annealing at 1000 K a bulk-truncated $p(2 \times 1)$ surface is found [with respect to a pure Pt(110) lattice]. According to the crystal structure two bulk terminations are possible (surface layer PtPt or PtSn), but exclusively mixed PtSn layers are exposed. Along the $[\bar{1}\bar{1}0]$ nearest-neighbor direction Sn and Pt atoms alternate, along $[001]$ all atoms in a row are either Sn or Pt. The described bulk termination by exclusively mixed layers agrees very well with the observation that all steps include even numbers of layers (double, quadruple steps, etc.). The $[00\bar{1}]$ steps, consisting of $\{102\}$ facets, tend to merge and form larger facets. As these facets were also found on $\text{Pt}_3\text{Sn}(001)$,²³ they seem to be energetically favorable in the Pt_3Sn system, in general. With the STM Sn atoms can not be resolved as protrusions among the Pt atoms since the local density of states at the Fermi edge is much lower for Sn than for Pt. This effect was seen on $\text{Pt}_3\text{Sn}(111)$ and (001) before and is agreement with band structure calculations.^{18,23,24}

In this study the $\text{Pt}_3\text{Sn}(110)$ alloy surface was oxidized following the same procedure as in the study of the (111) surface.¹¹ LEED afterwards showed an $c(4 \times 2)$ pattern, i.e., an additional $c(2 \times 2)$ superstructure with respect to the $p(2 \times 1)$ of $\text{Pt}_3\text{Sn}(110)$. STM images of the oxidized surface readily elucidate this structure. Large protrusions are observed, probably consisting of Sn-O aggregates. They are located in positions of a commensurate reconstruction on the substrate. Topographies of coexisting substrate and Sn-O phase regions show the protrusions above Sn positions. Equivalent but phase shifted adsorption sites give rise to domain structures separated by zigzag boundaries.

II. EXPERIMENTAL

The experiments were performed in an ultrahigh-vacuum (UHV) system at a base pressure below 5×10^{-11} mbar. The main features of the setup are an Omicron STM I system, a LEED system, and an 180° electrostatic analyzer for AES. For cleaning by sputtering and annealing the samples are transferred to a separate chamber. For sputtering a clean Ar^+ ion beam at an energy of 600 eV is used. The annealing temperature is monitored with a thermocouple.

Prior to oxidation experiments the sample was cleaned by sputtering and thermal annealing (1000 K) cycles. Initial carbon contamination of the sample was easily removed by oxygen treatment (10 min O_2 exposure at 5×10^{-6} mbar and 750 K sample temperature, and subsequent heating to 1150 K for further 5 min). For oxidation the $\text{Pt}_3\text{Sn}(110)$ surface was treated similar to the procedure applied in the $\text{Pt}_3\text{Sn}(111)$ case:¹¹ the clean sample was heated to temperatures in the range of 750–800 K and exposed to O_2 for typically several 10 min. The O_2 partial pressures were in the range of 1×10^{-6} mbar to 5×10^{-6} mbar, typical doses were in the range of several thousands of Langmuirs.

III. RESULTS

Before oxidation the clean $\text{Pt}_3\text{Sn}(110)$ sample exposes a $p(2 \times 1)$ LEED pattern (indexed with regard to the pure Pt

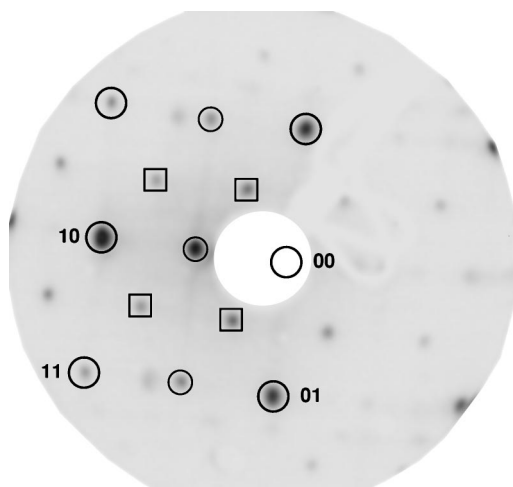


FIG. 1. LEED image of the oxidized $\text{Pt}_3\text{Sn}(110)$ surface (53.0 eV). The sample was exposed to 3400 L O_2 at 800 K. The additional spots are observed at $c(2 \times 2)$ positions (squares) with respect to the (2×1) pattern from the clean $\text{Pt}_3\text{Sn}(110)$ surface (marked by circles). Main spots as due to a pure Pt(110) surface are indexed, with respect to this lattice a $c(4 \times 2)$ pattern is seen.

lattice). After oxidation additional spots as shown in Fig. 1 occur. They are located at the centers of the rectangles formed by the preexisting spots, i.e., a $c(2 \times 2)$ superstructure with respect to the $p(2 \times 1)$ is observed. With respect to the Pt(110) lattice this is a $c(4 \times 2)$.

STM images as in Fig. 2 show that after oxidation the terraces are covered by large protrusions which can be recognized already in $(1000 \text{ \AA})^2$ frames. They are arranged in long-range ordered domains separated by clearly distinguishable zigzagged boundaries. Albeit these boundaries locally consist of segments running along $[\bar{1}\bar{1}\bar{1}]$ and $[\bar{1}\bar{1}1]$, their global direction is along $[\bar{1}\bar{1}0]$. Although the surface struc-

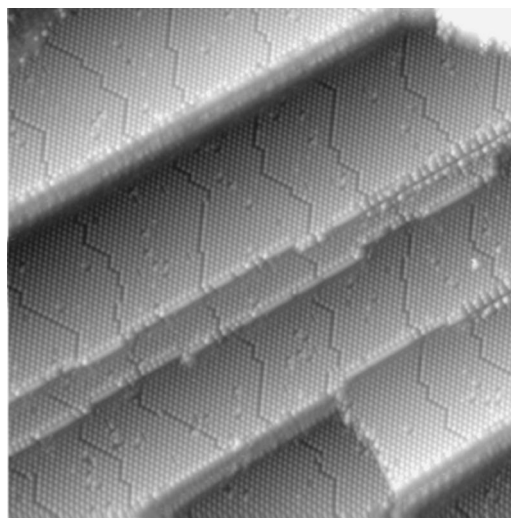


FIG. 2. STM overview $[(600 \text{ \AA})^2, U_T = +0.60 \text{ V}, I_T = 0.80 \text{ nA}]$ showing domains of large protrusions separated by boundaries running on the average in the $[\bar{1}\bar{1}0]$ direction. The sample was exposed to 2300 L O_2 at a sample temperature of 750 K.

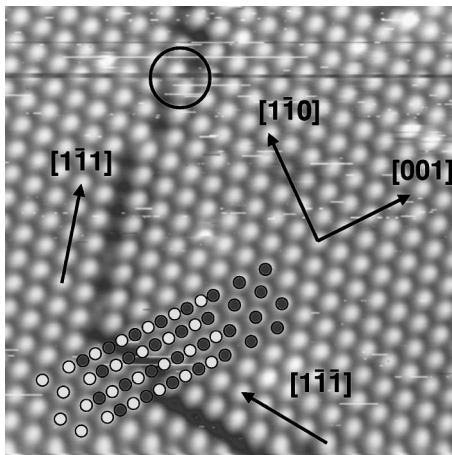


FIG. 3. STM image $[(120 \text{ \AA})^2]$, $U_T = +0.60 \text{ V}$, $I_T = 0.80 \text{ nA}$ of the oxidized phase with domain boundary. As indicated by the filled circles adjacent domains are shifted $1/2$ lattice constant in the $[001]$ direction (brighter circles: positions of circles in the left domain, darker circles: right domain). The open circle indicates protrusions within the domain boundary zone that are directly adjacent in the $[1\bar{1}0]$ direction.

ture is changed by oxidation still double (even number) steps with heights typical for the clean (110) are present. On these steps (along $[001]$ in fact $\{210\}$ minifacets) no protrusions are present. Therefore the thickness of the oxidation related surface region should not exceed one layer substantially. Slight variations of the oxidation parameters (temperatures 750–800 K, exposure 2000–4000 L) did not affect the LEED and STM results.

Figure 3 gives a closeup view of the surface after oxidation. The protrusions have a corrugation of about $0.7 \pm 0.2 \text{ \AA}$. Along $[001]$ as well as along $[1\bar{1}0]$ the next-neighbor distances of the protrusions are twice that of the respective values from the clean $p(2 \times 1)$. $[001]$ rows next to each other are shifted by half the protrusions distance. At domain boundaries the next protrusion along $[001]$ is located not two but three times the $p(2 \times 1)$ lattice constant away. Seemingly two equivalent but phase shifted adsorption sites exist, with all protrusions in a domain occupying the same superlattice. The shape and location of the protrusions in STM images did not depend on the tunneling parameters, only the corrugation was slightly influenced. Even at small tunneling voltages ($<0.1 \text{ V}$) stable tunneling was possible. At room temperature no mobility of the protrusions was observed.

On larger scale STM images often “dams” extending along $[001]$ are observed. Typically they are located at step edges (see Fig. 4). Their height is about $2\text{--}8 \text{ \AA}$, at the sides they exhibit the typical $\{210\}$ facets.

It is noteworthy that the step morphology is influenced by the oxidation. On the clean surface the $[001]$ steps tend to merge and form $\{210\}$ facets whereas the $[1\bar{1}0]$ steps basically meander perpendicular to the local slope of the crystal.²² After oxidation in both directions long straight double steps prevail, the terraces are basically all rectangular (see Figs. 4 and 5).

To determine the registry between the protrusions and the substrate the “oxide phase” was partially removed. This was

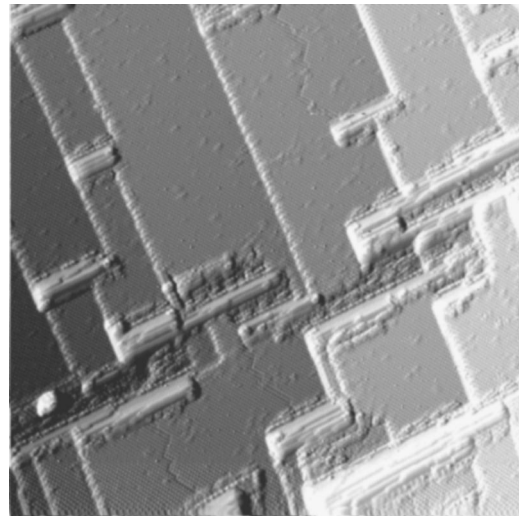


FIG. 4. STM image $[(1000 \text{ \AA})^2]$, $U_T = +0.60 \text{ V}$, $I_T = 0.80 \text{ nA}$ of the oxidized Pt₃Sn(110) surface. Mostly but not exclusively at the $[001]$ step edges “dams” occur that run parallel to the step.

accomplished by heating the oxidized surface shortly to temperatures between 900 and 940 K. AES measurements confirmed that during heating oxygen had begun to desorb from the surface. After cooling down to room temperature in the neighborhood of steps regions without protrusions were observed (see Fig. 5). Small scale STM topographs such as Fig. 6 show that these regions indeed exhibit the typical Pt₃Sn(110) $p(2 \times 1)$ substrate structure. The remaining “oxide protrusions” are still grouped in the typical domain structures. As evident, e.g., in Fig. 5, the protrusions are clearly located above Sn positions of the underlying substrate layer. Note that after the additional heating the dams described above have vanished (see discussion).

Thermal annealing at temperatures higher than 940 K leads to complete removal of the protrusions, then the com-

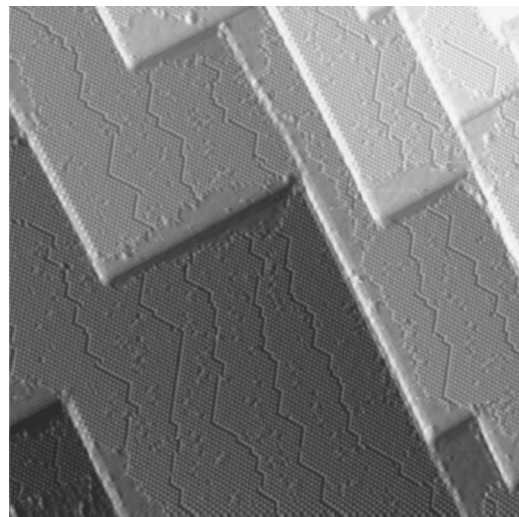


FIG. 5. STM topograph $[(800 \text{ \AA})^2]$, $U_T = +0.60 \text{ V}$, $I_T = 0.80 \text{ nA}$ after partial oxygen desorption. After cooling down to room-temperature regions without protrusions can be recognized at the steps.

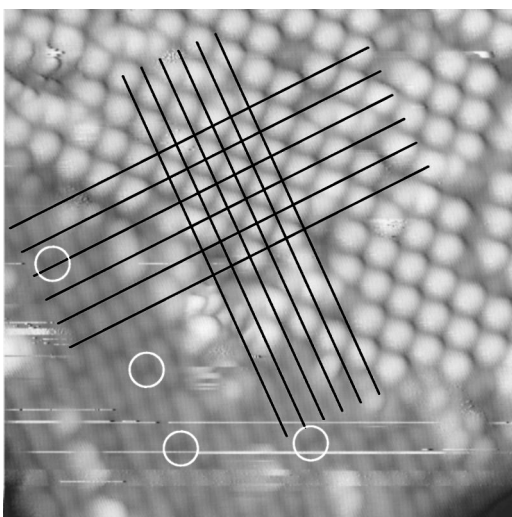


FIG. 6. STM topograph $[(100 \text{ \AA})^2]$, $U_T = +0.50 \text{ V}$, $I_T = 0.80 \text{ nA}$ after partial oxygen desorption. The regions without protrusions can be identified as $p(2 \times 1)$ substrate areas. To make this more obvious on the left side an inset with adopted gray scale is given. Here point defects at Sn positions appear, that are also known from the clean surface (white circles). As indicated by the lines the protrusions are located on top of Sn positions.

plete surface exhibits a $p(2 \times 1)$ substrate structure similar to before oxygen exposure. Thus oxidation can be revoked by thermal post annealing.

IV. DISCUSSION

From the STM observations the model in Fig. 7 that is consistent with all findings can be derived. The protrusions are located on top of Sn substrate atom, their spacing gives rise to a $c(2 \times 2)$ unit cell with respect to the $\text{Pt}_3\text{Sn}(110)$ $p(2 \times 1)$ substrate. This straightforwardly explains the LEED

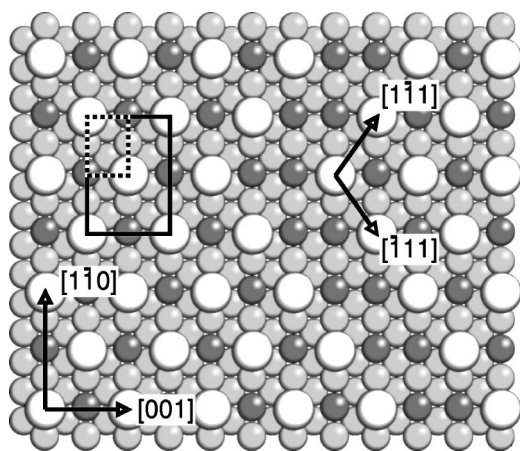


FIG. 7. Model of the (110) oxide structure with domain boundary. Light gray balls: Pt atoms, dark gray balls: Sn atoms, large white balls: location of the protrusions. Note that the protrusions probably consist of more than one atom. $p(2 \times 1)$ (dashed line) and $c(4 \times 2)$ [$c(2 \times 2)$ of the $p(2 \times 1)$] (solid line) unit cells and the relevant directions are indicated.

patterns. Note that the given model makes no assertions with respect to the protrusions inner structure but only on their registry relative to the substrate as it is not possible to determine the precise nature of the protrusions directly from the STM images. No inner structure was observable, in all STM images the protrusions appear as uniform entities. In all known studies of the oxidation of Pt-Sn surfaces afterwards the outermost surface layer(s) consisted merely of Sn and O,^{5-8,10,11,13-17} in agreement with the strong affinity of Sn toward O. Taking the large corrugation of $\approx 0.7 \text{ \AA}$ and diameter of $> 6.0 \text{ \AA}$ of the protrusions into account, they probably do not correspond to single atoms. However, during the further discussion the protrusions will be regarded as enclosed entities if not indicated otherwise. This allows a concise description of the observed Sn-O phase properties.

As evident from STM topographs such as Fig. 6 upon partial desorption the oxide is limited to one or very few atomic layers, it can be regarded as a two-dimensional ultra-thin film. The nearest neighbors of a protrusion are located 6.9 \AA distant in the $\langle 1\bar{1}\bar{1} \rangle$ direction, the next nearest at 8.0 \AA along $\langle 001 \rangle$. This structure might be interpreted as compressed pseudohexagonal grid. Remarkably the protrusions stick together in domains of this kind, even if they could spread out onto uncovered substrate areas (see Fig. 5). On the other hand, smaller distances between protrusions are hardly ever seen. Exceptions occur in kinks within the domain boundaries where protrusions are separated only 4.0 \AA along $[1\bar{1}0]$ (see Fig. 3). Treating the protrusions as entities it seems that longer-range attractive forces glue the protrusions together while shorter-range repulsive forces hinder denser structures.

As in the oxide structure only every second Sn substrate atom is covered by a protrusion, two equivalent but phase-shifted adsorption superlattices exist. This gives rise to the observed two domain structure. In the domain boundaries the nearest protrusion along $[001]$ is located not on the second but third next Sn atom. All domain boundaries consist locally of $[1\bar{1}\bar{1}]$ and $[1\bar{1}1]$ segments, what coincides with the nearest-neighbor directions. This is consistent with the hypothetical attractive interactions between protrusions: in the $[1\bar{1}\bar{1}]$ and $[1\bar{1}1]$ segments the number of nearest neighbors (3) of boundary protrusions is maximized in comparison to, e.g., $[1\bar{1}0]$ (2).

On a larger scale every domain runs more or less parallel to the $[1\bar{1}0]$ direction. Even taking the preference for $[1\bar{1}\bar{1}]$ and $[1\bar{1}1]$ segments into account many alternative structures could occur, e.g., zigzag boundaries running parallel to $[001]$ or rhomboidal domains, but such are never seen. A possible explanation for this preferred $[1\bar{1}0]$ orientation could be a strain relief mechanism: Usually strain is accumulated in the surface, which is altered by adsorbates. The (110) surface is highly anisotropic and uniaxial strain could result from the adsorbed oxygen layer. Relief could be obtained when the layer breaks up in stripe domains along one direction, in this case $[1\bar{1}0]$. In this context, it is worth mentioning that on the uncovered $\text{Pt}_3\text{Sn}(111)$ a subsurface dislocation network serves to relieve stress and gives rise to a mesoscopic hon-

eycomb network.¹⁸ However, in this case, no direct evidence for a stress relief mechanism is obtained. Note that (a) only obtuse angles between $[1\bar{1}\bar{1}]$ and $[1\bar{1}\bar{1}]$ segments occur and (b) domain boundaries never intersect. Again a tendency to maximize the number of neighbors could explain why obtuse angles are more favorable than sharp angles: the in plane coordination of the most exposed protrusion is identical (2), but there is a next-nearest neighbor (along $[001]$) in an obtuse angle whereas in a sharp angle there is not. This would inhibit intersections as well. In principle the structures with “very near” protrusions along $[1\bar{1}\bar{0}]$ could give an acute angle with higher coordination, but that is never seen. Given this preference for obtuse angles and provided that $[1\bar{1}\bar{1}]$ and $[1\bar{1}\bar{1}]$ segments have similar length distributions (as expected for symmetry reasons), the average $[1\bar{1}\bar{0}]$ orientation is plausible.

Oxygen exposure also affects the step morphology. Especially the $[1\bar{1}\bar{0}]$ steps, on the clean Pt₃Sn(110) surface curving perpendicular to the local surface slope,²² become long and straight. The Sn-O layers stabilize the steps, possibly because kinks become unfavorable. However, these substrate steps do not coincide with the $[1\bar{1}\bar{1}]$ and $[1\bar{1}\bar{1}]$ directions preferred for domain boundaries. Note that in the STM images obtained after partial oxygen desorption by additional heating (see Fig. 5) the regions free of the Sn-O phase are located at the steps. This can be explained by low coordinated protrusions at the steps being weaker bound and desorbing first. However, desorption takes place at high temperatures when there is an increased mobility in the surface. Thus the protrusions as well could have aggregated into the observed closed domains only during cooling down. Room-temperature STM cannot give information on the actual desorption process.

Another detail of the oxidized surface to be discussed are the dams seen after oxidation (see Fig. 3). The clean Pt₃Sn(110) is after sputtering and annealing at 600 K quite rough with many $\{210\}$ facets.²² Even after annealing at 1000 K (applied during the cleaning period before oxygen exposure) some ripples of the hill-and-valley structure remain. As the “dams” show the same general direction and the same preference for $\{210\}$ facets, the dams are likely just remnants of such preexisting ripples. This assumption is supported by the fact that the “dams” disappear after further post annealing. The prevalent location of the dams at step edges might be due to pinning of the terraces at these structures.

V. COMPARISON WITH THE OXIDATION OF THE Pt₃Sn(111) SURFACE

Although the dense packed Pt₃Sn(111) and the open (110) surfaces have completely different geometric structures, the phases formed upon oxygen exposure at sample temperatures of about 750 K show many common properties. In both cases only thin, two-dimensional overlayers are formed. STM topographs show large, spherical protrusions. Their inner structure is unsolved, but they probably do not simply correspond to single adsorbed atoms.

On both (111) and (110) the protrusions are arranged in commensurate superlattices with lattice constants twice as large as the substrates. In both cases simple LEED superstructures are observed. The (111) Sn-O phase has *a priori* a hexagonal structure, the (110) Sn-O overlayer can be interpreted as pseudohexagonal. The next-neighbor distances are of the same order of magnitude, with the (111) distance (5.66 Å) about 80% of the (110) value (6.92 Å). In the Pt₃Sn(111) Sn-O (4×4) phase every second protrusion in every second row is missing, the distance of the remaining protrusions is increased by the formation of zigzag patterns.¹¹ If one thinks of these protrusions as closed entities, repulsive interactions becoming important at shorter distances could account for these observations. However, such a description is not in line with the recent results from LEED *I-V* studies.¹² On the (110), where next-neighbor distances are larger, such a (4×4) reconstruction is not observed.

Whereas on (110) domain structures occur, on the (111) comparable boundaries were never observed. If on the (111) phase shifted adsorption lattices existed, they should also give rise to domains, but no domain boundary structures were found. On both surfaces after oxygen exposure the step morphologies changed, low-index steps are stabilized. It can be speculated that Sn-O domains located above or below impose energetical favorable directions on the steps, wandering kinks get expelled.

When the Sn-O phase was partially removed, on both surfaces the protrusions form closed islands indicative of attractive interactions. The temperature at which partial desorption took place [>940 K for the (110) and >1050 K for the (111)] was higher for the (111). Thus the Sn-O phase seems to be slightly more stable on the (111). On both surfaces after oxygen desorption the substrate as it was before oxygen exposure was restored.

Considering all these similarities probably other results from the (111) hold for the (110) surface as well. XPS and LEIS indicated for the (111) that after complete oxidation Pt was no longer present in the outermost layers, but only in the subsurface region. This is in agreement with all known studies of polycrystalline Pt₃Sn and Sn-Pt surface alloys.^{5-8,13-17} Thus it is safe to assume that the (110) protrusions likewise do not contain Pt but only Sn-O. XPS on oxidized Pt₃Sn (111) gave no evidence for the formation of a SnO_x oxide phase, instead an Sn-O phase with chemisorbed oxygen was proposed. As the (110) Sn-O layer is ultrathin as on the (111), it can be speculated that again no real oxide is formed. In Fig. 6 the protrusions appear as ad features on the substrate, but this might be misleading as the sample was heated to obtain the partly desorbed termination. Without further information STM can not determine the subsurface region structure. It cannot be excluded that these regions differ from the bulk and that the apparent $p(2 \times 1)$ substrate region has undergone a rearrangement during oxygen desorption.

It is remarkable that the Sn-O protrusions look that similar on Pt₃Sn(111) and (110). The geometric structure of the substrate has if at all only a weak influence on the appearance of the protrusions. Thus electronic effects should be more important in this case. As no inner structure of the protrusions is visible, the STM can give no further informa-

tion. However, a recent tensor LEED analysis of the Pt₃Sn(111)-O system gave the best agreement between measured and simulated *I-V* curves for a model in which the protrusions correspond to tin atoms occupying on-top positions.¹² Oxygen adsorbed on metal surfaces is imaged in STM typically as depression [e.g., fcc bonded atomic oxygen on a Pt(111)^{25,26}], but sometimes also as protrusion [bridge-bonded atomic oxygen on Pt(110) or stepped Pt(111)^{27,28}]. In the given system the situation is even more complicated, as apparently the interaction with other Sn or O atoms inhibits the imaging of separate oxygen atoms. The observed structures on both (111) and (110) can be described as adsorbate structures of “pseudomolecules” attracting or repelling each other. Maybe within the protrusions the bond between Sn and O is quite strong, charge transfer effects might give rise to the interactions. On the other hand, mere spatial hindrance is also possible. Batzill *et al.* observed on Sn/Pt(111) surface alloys under certain oxidation conditions a (4×4) reconstruction similar to O-Pt₃Sn(111) (4×4).¹⁷ This structure was interpreted as an “adsorption of SnO pseudomolecules at preferential sites.”

The formation of Sn-O overlayers is interesting from a technological point of view. Solid-state gas sensors based on SnO₂ are of big importance,⁴ and platinum was found to promote the selectivity and sensitivity of such sensors.²⁹ However, these gas sensors rely on the existence of a band gap, in which molecules chemisorbed on the surface may induce “extrinsic” electronic states. On both the studied Pt₃Sn single crystal surfaces the formed Sn-O layers were very thin and in XPS showed [for the (111)] no bulk properties of SnO_x oxides. STM indicated that the overlayers on both Pt₃Sn(111) and (110) exhibit metallic behavior. The properties of these ultrathin Sn-O layers are governed by the metallic substrate, they are very likely not suitable as gas sensors.

VI. SUMMARY

The adsorption of oxygen on the Pt₃Sn(110) alloy surface was studied by means of STM and LEED. After exposure to 2300 L O₂ at 750 K STM topographs show a thin layer of

large protrusions. Their arrangement in a commensurate pseudohexagonal lattice gives rise to a LEED pattern with additional $c(2\times 2)$ spots with regard to the substrate $p(2\times 1)$ pattern, i.e., a $c(4\times 2)$ with respect to the Pt lattice. Domain structures occur due to two equivalent phase-shifted adsorption lattices of the adlayer on the substrate. All domain boundaries, consisting locally of $[1\bar{1}\bar{1}]$ and $[1\bar{1}1]$ segments, run more globally in $[1\bar{1}0]$ direction. This morphology can be explained assuming that (a) it is favorable for the protrusions to maximize the number of nearest and next-nearest neighbors and (b) neither of the $[1\bar{1}\bar{1}]$ and $[1\bar{1}1]$ directions is preferred over each other. By post annealing to less than 940 K it was possible to prepare adlayer domains coexisting with substrate regions. STM then revealed that the protrusions are located above Sn locations. Further post annealing at more than 940 K removed the adlayer completely, the clean Pt₃Sn(110) substrate was restored. A model of the adlayer structure is given that is consistent with all STM and LEED findings.

The described structures obtained by oxygen exposure have many similar properties as structures obtained on Pt₃Sn(111) under similar conditions. In accordance with the (111) LEIS/XPS results and all known other studies of the oxidation of Pt₃Sn surfaces the (110) protrusions very probably consist only of Sn and O, not Pt. Their appearance in the STM is likely determined by electronic effects. As similar protrusions are likewise observed on the (111), they could act as topographic indicators for the Sn-O phase. Albeit XPS results from the oxidation of Pt₃Sn(111) indicate no SnO_x oxide formation, but chemisorbed oxygen, the STM observations can most easily interpreting the protrusions as interacting Sn-O clusters.

ACKNOWLEDGMENTS

This work was supported by the Deutsche Forschungsgemeinschaft (DFG), the Nederlandse Organisatie voor Wetenschappelijk Onderzoek (NWO), the Stichting voor Fundamenteel Onderzoek der Materie (FOM) and the MURST under the program “Crescita, struttura e reattività di superfici di materiali e di film superficiali.”

*Electronic address: speller@sci.kun.nl

¹F. M. Dautzenberg, J. N. Helle, P. Biloen, and W. M. H. Sachtler, *J. Catal.* **63**, 119 (1980).

²K. Wang, H. A. Gasteiger, N. M. Markovic, and P. N. Ross, Jr., *Electrochim. Acta* **41**, 2587 (1996).

³C. Panja, N. Saliba, and B. E. Koel, *Surf. Sci.* **395**, 248 (1998).

⁴W. Goepel and K. D. Schierbaum, *Sens. Actuators B* **26-27**, 1 (1995).

⁵G. B. Hoflund, D. A. Asbury, P. Kirszenstejn, and H. A. Laitinen, *Surf. Sci.* **161**, L583 (1985).

⁶G. B. Hoflund, D. A. Asbury, P. Kirszenstejn, and H. A. Laitinen, *Surf. Interface Anal.* **9**, 169 (1986).

⁷G. B. Hoflund and D. A. Asbury, *Langmuir* **2**, 695 (1986).

⁸D. A. Asbury and G. B. Hoflund, *Surf. Sci.* **199**, 552 (1988).

⁹S. D. Gardner, G. B. Hoflund, and D. R. Schryer, *J. Catal.* **119**, 179 (1989).

¹⁰W. Unger and D. Marton, *Surf. Sci.* **218**, L467 (1989).

¹¹M. Hoheisel, S. Speller, W. Heiland, A. Atrei, U. Bardi, and G. Roviada, *Phys. Rev. B* **66**, 165416 (2002).

¹²A. Atrei, U. Bardi, G. Roviada, M. Torrini, M. Hoheisel, and S. Speller, *Surf. Sci.* **526**, 193 (2003).

¹³N. A. Saliba, Y.-L. Tsai, and B. E. Koel, *J. Phys. Chem. B* **103**, 1532 (1999).

¹⁴D. I. Jerdev and B. E. Koel, *Surf. Sci.* **492**, 106 (2001).

¹⁵M. Batzill, D. E. Beck, D. Jerdev, and B. E. Koel, *J. Vac. Sci. Technol. A* **19**, 1953 (2001).

- ¹⁶M. Batzill, D. E. Beck, and B. E. Koel, *Appl. Phys. Lett.* **78**, 2766 (2001).
- ¹⁷M. Batzill, D. E. Beck, and B. E. Koel, *Phys. Rev. B* **64**, 245402 (2001).
- ¹⁸J. Kuntze, S. Speller, W. Heiland, A. Atrei, I. Spolveri, and U. Bardi, *Phys. Rev. B* **58**, R16 005 (1998).
- ¹⁹A. Haner, P. Ross, and U. Bardi, *Catal. Lett.* **8**, 1 (1991).
- ²⁰U. Bardi, L. Pedocchi, G. Rovida, A. N. Haner, and P. N. Ross, in *Fundamental Aspects of Heterogenous Catalysis Studied by Particle Beams*, edited by H. H. Brongersma and R. A. van Santen (Plenum Press, New York, 1991), pp. 393–397.
- ²¹A. N. Haner, P. N. Ross, and U. Bardi, in *The Structure of Surfaces III*, edited by S. Y. Tong, M. A. Van Hove, K. Takayanagi, and X. D. Xie, Vol. 24 of *Springer Series in Surface Science* (Springer Verlag, Berlin, 1991), pp. 276–281.
- ²²M. Hoheisel, S. Speller, J. Kuntze, A. Atrei, U. Bardi, and W. Heiland, *Phys. Rev. B* **63**, 245403 (2001).
- ²³M. Hoheisel, J. Kuntze, S. Speller, A. Postnikov, W. Heiland, I. Spolveri, and U. Bardi, *Phys. Rev. B* **60**, 2033 (1999).
- ²⁴Š. Pick, *Surf. Sci.* **436**, 220 (1999).
- ²⁵J. Wintterlin, R. Schuster, and G. Ertl, *Phys. Rev. Lett.* **77**, 123 (1996).
- ²⁶P. Sautet, *Surf. Sci.* **374**, 406 (1997).
- ²⁷E. Janin, H. von Schenck, M. Göthelid, U. O. Karlsson, and M. Svensson, *Phys. Rev. B* **61**, 13 144 (2000).
- ²⁸P. J. Feibelman, S. Esch, and T. Michely, *Phys. Rev. Lett.* **77**, 2257 (1996).
- ²⁹C.-H. Shim, D.-S. Lee, S.-I. Hwang, M.-B. Lee, J.-S. Huh, and D.-D. Lee, *Sens. Actuators B* **81**, 176 (2002).